The Atlantic Multidecadal Variability Phase Dependence of Teleconnection between the North Atlantic Oscillation in February and the Tibetan Plateau in March🖉

Jingyi Li,[a,b] Fei Li,[c,b] Shengping He,[c,b] Huijun Wang,[b,d,e] and Yvan J Orsolini[f]

[a] *Nanjing Institute of Geography and Limnology, Chinese Academy of Sciences, Nanjing, China*
[b] *Collaborative Innovation Center on Forecast and Evaluation of Meteorological Disasters/Key Laboratory of Meteorological Disaster, Ministry of Education, Nanjing University of Information Science and Technology, Nanjing, China*
[c] *Geophysical Institute, University of Bergen and Bjerknes Centre for Climate Research, Bergen, Norway*
[d] *Climate Change Research Center, Chinese Academy of Sciences, Beijing, China*
[e] *Nansen-Zhu International Research Center, Institute of Atmospheric Physics, Chinese Academy of Sciences, Beijing, China*
[f] *NILU-Norwegian Institute for Air Research, Kjeller, Norway*

ABSTRACT: The Tibetan Plateau (TP), referred to as the "Asian water tower," contains one of the largest land ice masses on Earth. The local glacier shrinkage and frozen-water storage are strongly affected by variations in surface air temperature over the TP (TPSAT), especially in springtime. This study reveals that the relationship between the February North Atlantic Oscillation (NAO) and March TPSAT is unstable with time and regulated by the phase of the Atlantic multi-decadal variability (AMV). The significant out-of-phase connection occurs only during the warm phase of AMV (AMV+). The results show that during the AMV+, the negative phase of the NAO persists from February to March, and is accompanied by a quasi-stationary Rossby wave train trapped along a northward-shifted subtropical westerly jet stream across Eurasia, inducing an anomalous adiabatic descent that warms the TP. However, during the cold phase of the AMV, the negative NAO cannot persist into March. The Rossby wave train propagates along the well-separated polar and subtropical westerly jets, and the NAO–TPSAT connection is broken. Further investigation suggests that the enhanced synoptic eddy and low-frequency flow (SELF) interaction over the North Atlantic in February and March during the AMV+, caused by the southward-shifted storm track, helps maintain the NAO pattern via positive eddy feedback. This study provides a new detailed perspective on the decadal variability of the North Atlantic–TP connection in late winter to early spring.

KEYWORDS: Atmosphere-ocean interaction; Eddies; Feedback; Rossby waves; Teleconnections

1. Introduction

The Tibetan Plateau (TP) is known as the "Asian water tower" because it has the most glaciers outside the polar regions and acts as a dominant water supply source for 2 billion people downstream in South and East Asia (Xu et al. 2008, 2014; Yao et al. 2012). The high elevation makes the TP particularly vulnerable to climate change (Liu and Chen 2000; Palazzi et al. 2017; Pepin et al. 2015) through snow albedo (Imtiaz et al. 2009), cloud (Yan et al. 2018), and aerosol (Su et al. 2018; Ramanathan and Carmichael 2008) feedbacks. In recent decades, the TP has experienced faster annual warming rates than the global average (approximately $0.12°C \, decade^{-1}$ for 1951–2012; IPCC 2014), with a value of approximately $0.16°C \, decade^{-1}$ in 1955–96 (Liu and Chen 2000; Wang et al. 2008). While the TP snow accumulation peaks in late winter, a rise in TP temperature in spring further results in a decrease in regional snow depth, glacier retreat, and delayed phenology (Maurer et al. 2019; Yu et al. 2010; Gao et al. 2012). Furthermore, long-lasting snow-depth anomalies could persist into

summer, impacting surface air temperature over the TP (TPSAT), disturbing the western Pacific subtropical high, and modulating precipitation over East Asia (Wu and Qian 2003; Zhang et al. 2004; Zhu et al. 2008). As the increase in the TP annual temperature is predicted to continue, extreme temperature and precipitation events could become more frequent, with consequential impacts downstream (Guo et al. 2016; Li et al. 2010; Bao et al. 2010).

Previous studies have suggested that TPSAT variability in winter and early spring is closely tied to the variation in extratropical atmospheric circulations, including Rossby waves and the westerly jet stream. In the Euro–Atlantic sector, quasi-stationary Rossby wave trains (RWTs) could propagate across Eurasia along two waveguides: the subtropical westerly jet stream and the polar-front jet stream, disturbing circulations over the TP (Li et al. 2005). Bao and You (2019) stated that the weakened and northward-shifted East Asian subtropical jet over the TP, generally concurrent with an anomalous high that weakens the India-Myanmar trough, induces an anomalous descending motion above the TP via secondary circulations and hence significant atmospheric warming through anomalous adiabatic heating.

The North Atlantic Oscillation (NAO), as the most prominent internal atmospheric variability pattern over the North Atlantic on a monthly time scale (Hurrell 2003), has been shown to excite RWTs in the subtropical route (Watanabe 2004) and also in the subpolar route (Li et al. 2008) especially during late winter and early spring, which is attributable to the
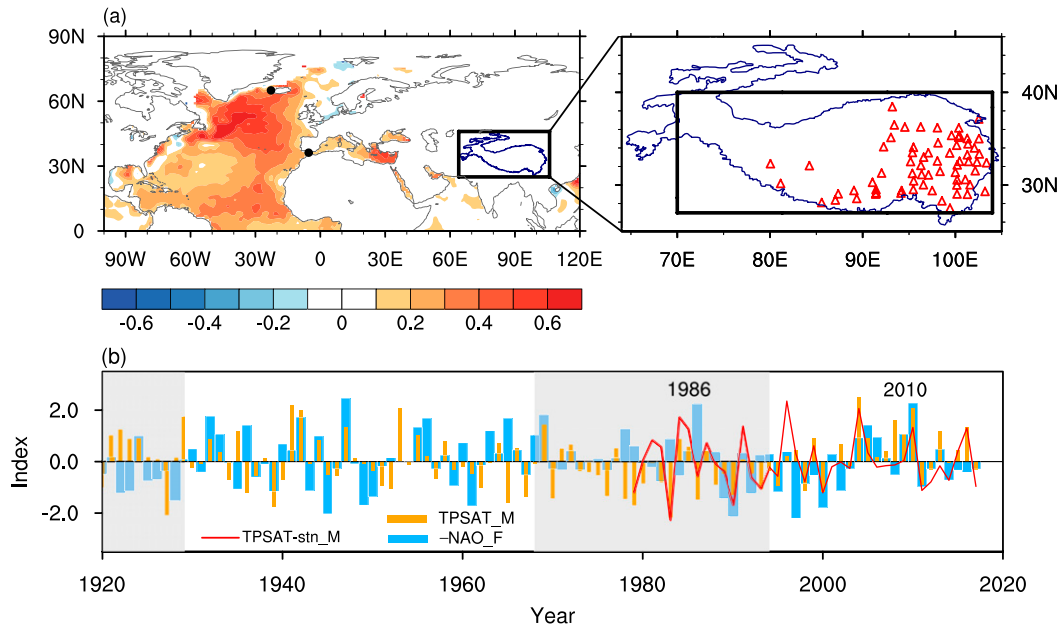
FIG. 1. (a) Composite difference of SST (shading; °C) in February–March between the warm and cold AMV phases and distribution of observation stations (red triangles) located above 2600 m above mean sea level in the TP used in this study. Black points denote the stations of Gibraltar (36.2°N, 5.4°W) and southwest Iceland (65°N, 22.8°W). (b) Negative NAO index in February (blue bars) and March TPSAT index derived from CRU (orange bars) in 1920–2017 and from station observation (red line) in 1979–2017. Gray stripes denote the periods of the cold AMV phase.

enhanced convergence variability over the Mediterranean Sea that favors Rossby wave propagation (Watanabe 2004). Consequently, the negative-phase NAO (NAO−) is found to increase simultaneous TPSAT by weakening the East Asian subtropical jet and enhancing the descending motion over the TP (Xin et al. 2010; You et al. 2011). In turn, anomalous TP warming could shift the overlying westerly more northward by changing the meridional temperature gradient, serving as a positive feedback on atmospheric circulation (Chen et al. 2020). Furthermore, Li et al. (2005) linked the March TPSAT to the precursory December–February NAO through changes in the subtropical westerly jet stream across Eurasia. However, since the NAO harbors distinct subseasonal variability in winter and spring, the dynamic processes by which the NAO subseasonal changes or its persistence impacts the circulation and temperature over the TP remain to be fully elucidated.

Moreover, the Atlantic multidecadal variability (AMV), the major multidecadal oceanic pattern with its warm phase (i.e., AMV+) characterized by positive SST anomalies across the North Atlantic basin (Kerr 2000; Zhang et al. 2019; Fig. 1a), is found to have potential modulation upon NAO signals in late winter/early spring. During the AMV+, the warmer ocean releases more energy toward the air via enhanced upward turbulent heat fluxes over the Gulf Stream, disturbing the overlying atmospheric baroclinicity and shifting the storm track more southward (Peings and Magnusdottir 2014; Ruprich-Robert et al. 2017). The transient eddy feedback caused by the altered Atlantic storm track projects an NAO−-like pattern in the large-scale circulations. In the upper troposphere, the subtropical jet stream over the North

Atlantic accelerates, while the polar-front jet stream decelerates and moves equatorward (Msadek et al. 2010). In addition, a recent study noted that the AMV could modulate the unstable connection between El Niño–Southern Oscillation (ENSO) and the NAO in late winter by intensifying or obscuring ENSO-related SST anomalies (Zhang et al. 2018). However, although Shen et al. (2011) revealed an out-of-phase correlation between long-term snow proxy records over the TP derived from ice cores and the AMV conveyed by the NAO, the underlying mechanisms were not discussed.

It is acknowledged that during winter, the monthly NAO− is associated with a decelerated subtropical jet and polar-front jet over the North Atlantic, which forms a southward-shifted Atlantic storm track (Hoskins et al. 1983; Hurrell 2003). The concurrent synoptic eddy and low-frequency flow (SELF) interaction plays an important role in the persistence of the NAO flow, suggestive of positive feedback from transient eddies (Pan and Jin 2005; Ren et al. 2012). Interestingly, the basic mechanisms of the decadal AMV also involve an interaction between the time-mean flow and the altered Atlantic storm track, which further motivates us to investigate the combined effects from the NAO and the AMV on the TP climate.

In the following content, section 2 introduces the data and methods employed in this study. Section 3 includes the observed unstable NAO–TPSAT connection in late winter to early spring (section 3a), the atmospheric circulation response to the February NAO during different AMV phases (section 3b), and the modulation of the AMV upon SELF feedback to the NAO flow (section 3c). The discussion and summary are presented in section 4.

2. Data and methods

a. Data and climate indices

This study makes use of six datasets. 1) The monthly sea level pressure (SLP) data with $5° × 5°$ resolution for 1850–2017 are derived from Met Office Hadley Centre HadSLP2r data (Allan and Ansell 2006). 2) The monthly SAT data with $0.5° × 0.5°$ resolution for 1901–2017 are derived from Climatic Research Unit (CRU) TS 3.26 data (Harris et al. 2014). 3) The daily station-based SAT data for 1979–2017 comprise records from 67 Chinese Meteorological Administration stations located above 2600 m above mean sea level in the TP (denoted by the red triangles in Fig. 1a), provided by the National Climate Center, Chinese Meteorological Administration. 4) and 5) The daily and monthly atmospheric data, including geopotential height, winds, and temperature with $2° × 2°$ resolution, are derived from the European Centre for Medium-Range Weather Forecasts (ECMWF) twentieth-century reanalysis (ERA-20C; 1900–2010; Poli et al. 2016) and interim reanalysis (ERA-Interim; 1979–2017; Dee et al. 2011). 6) SST data are derived from the Met Office Hadley Centre with $1° × 1°$ resolution for 1870–2018 (Rayner et al. 2003).

The monthly NAO index used here is defined as the SLP difference between the stations in Gibraltar and in southwest Iceland (Jones et al. 1997; Fig. 1a: black points), provided by CRU (https://crudata.uea.ac.uk/cru/data/nao/). The TPSAT index used in this work is defined as SAT anomalies averaged over 27°–40°N, 70°–104°E (indicated by the rectangle in Fig. 1a) derived from CRU. The station-based TPSAT index is calculated as the weighted average of the 67 stations. Linear trends have been removed from the above-mentioned indices and fields. The annual-mean AMV index of 1890–1999 is the same as in Ting et al. (2009), defined as the internal component of SST variability averaged over 0°–60°N, 7.5°–75°W with a low-pass filter of a 10-yr cutoff. The internal component is the residual of observed SST subtracting the external forced component dominated by anthropogenic forcing, while the forced component is estimated by a suite of IPCC Climate of the Twentieth Century(C20C) coupled model simulations applying a signal-to-noise maximizing empirical orthogonal function analysis. Additionally, this index suggests that the AMV turns to its warm phase in the 1990s and starts its downturn in early 2010s (Ruprich-Robert et al. 2017). In this study, the warm AMV phase denotes periods with the AMV index above zero (i.e., 1930–68 and 1995–2017), whereas the cold AMV phase denotes periods with the AMV index below zero (i.e., 1920–29 and 1969–94).

b. Methods

In this study, the analyses are based on a patched dataset with a period of 1920–2017, which combines ERA-20C and ERA-Interim (1920–78 from ERA-20C and 1979–2017 from ERA-Interim), in order to cover the latest data and to improve data accuracy especially for daily data. To test the robustness, some diagnostics are repeated in the online supplemental material using only ERA-20C over the period 1920–2010. Lead–lag correlation of the monthly CRU TPSAT index with the NAO index from November to March in 1920/21–2016/17 is first calculated to clarify the precedence of winter NAO.

Significant negative correlation only exists between February NAO and March TPSAT with a correlation efficient of -0.24 (over the 95% confidence level), indicative of a North Atlantic–TP teleconnection in late winter to early spring. This study hence focuses on the unstable relationship between February NAO and March TPSAT.

The climatological westerly jet is represented as the maxima of the 250-hPa westerlies. To give more details on the stationary Rossby wave propagation, the wave activity flux (WAF) is introduced based on Takaya and Nakamura (2001). The Eady growth rate is given by $\sigma_E = 0.3098|f||\partial u(z)/\partial z|/N$ (Vallis 2006), where f is the Coriolis parameter, $u(z)$ is the vertical profile of the westerly winds, z is the vertical coordinate, and N is the buoyance frequency[(where $N^2 = (g/\theta)(\partial\theta/\partial z)$, in which g and θ are gravitational acceleration and potential temperature, respectively].

Transient eddy activity is computed as the root-mean-square of daily bandpass-filtered geopotential height with periods of 2.5 to 6 days (Lau and Nath 1991), that is, $\left(\overline{H'^2}\right)^{1/2}$ (the prime and overbar hereafter represents transient perturbation and monthly average, respectively). Localized Eliassen–Palm (E-P) flux is introduced to illustrate eddy forcing of the zonal mean flow (Hoskins et al. 1983; Trenberth 1986), calculated as $\mathbf{E} = (1/2)(\overline{v'^2} - \overline{u'^2})\mathbf{i} - \overline{u'v'}\mathbf{j}$, where u and v are zonal and meridional winds, respectively, while $\mathbf{i}$ and $\mathbf{j}$ are the zonal and meridional axes. The divergence of $\mathbf{E}$ indicates the eddy-induced acceleration of zonal winds through barotropic processes and vice versa. Generally, divergent westerly $\mathbf{E}$ vectors appear along the storm track, which act to accelerate the westerly mean flow in situ (Lau 1988; Figs. 10d,e).

3. Results

a. The unstable NAO–TPSAT connection in late winter to early spring

The temporal evolutions of the negative February NAO index and March TPSAT indices based on CRU (1920–2017) and in situ stations (1979–2017) are illustrated first (Fig. 1b). Although derived from independent data resources (since CRU does not include station data over the TP), the two TPSAT indices compare well with each other for 1979–2017 (Corr.= 0.84, over the 99% confidence level). The March TPSAT shows more frequent in-phase variation with the February NAO− during the AMV+ than the cold AMV phase (AMV−; gray shading in Fig. 1b). This result is quantitatively supported by Fig. 2, which illustrates the 31-yr running correlation between the February NAO− and March TPSAT, together with the temporal evolution of the annual mean AMV. As expected, their correlation is unstable: it is statistically significant (over the 95% confidence level) over approximately the 1930s–60s and 1990s–2010s (i.e., AMV+ periods), but it is insignificant and even changes signs in other periods (i.e., AMV− periods). On average, the correlation coefficient of the negative February NAO index and March TPSAT index during the AMV+ is 0.37 (over the 99% confidence level), while that during the AMV− is −0.03 (insignificant). These results thus motivate us to categorize the entire analysis period into two
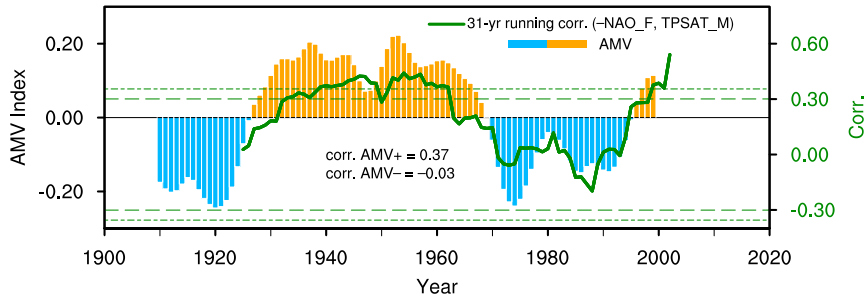
FIG. 2. Annual-mean AMV index from 1910 to 1999 (bars) and running correlation in a 31-yr moving window between the negative February NAO index and March TPSAT index (line). The 90% and 95% confidence levels for the correlations are indicated by the horizontal dashed and dotted green lines, respectively.

subperiods based on the AMV phases in the following analysis to explore the diverse dynamic processes during each phase.

b. The atmospheric circulation response to February NAO− during different AMV phases

Figure 3 illustrates the February and March SLP regressions upon the negative February NAO index during the two AMV phases. In February, during both AMV+ and AMV−, one finds a typical NAO−-related meridional-dipole pattern, with a primary maximum over Iceland and a minimum over the midlatitude North Atlantic (Fig. 3: contours). However, the

March SLP anomaly shows a significant difference. During the AMV+, the meridional dipole pattern established by February largely persists into March, indicative of a 2-month duration of the NAO− (Fig. 3a: shading). During the AMV−, however, the March SLP anomalies are much weaker and localized eastward, with a maximum over the Urals and a minimum over the eastern North Atlantic (Fig. 3b: shading), suggesting the downstream movement of circulation anomalies in March.

The different circulation responses to the February NAO− shown in Fig. 3 inspire us to compare atmospheric characteristics in March based on the AMV phases. During the AMV+, there
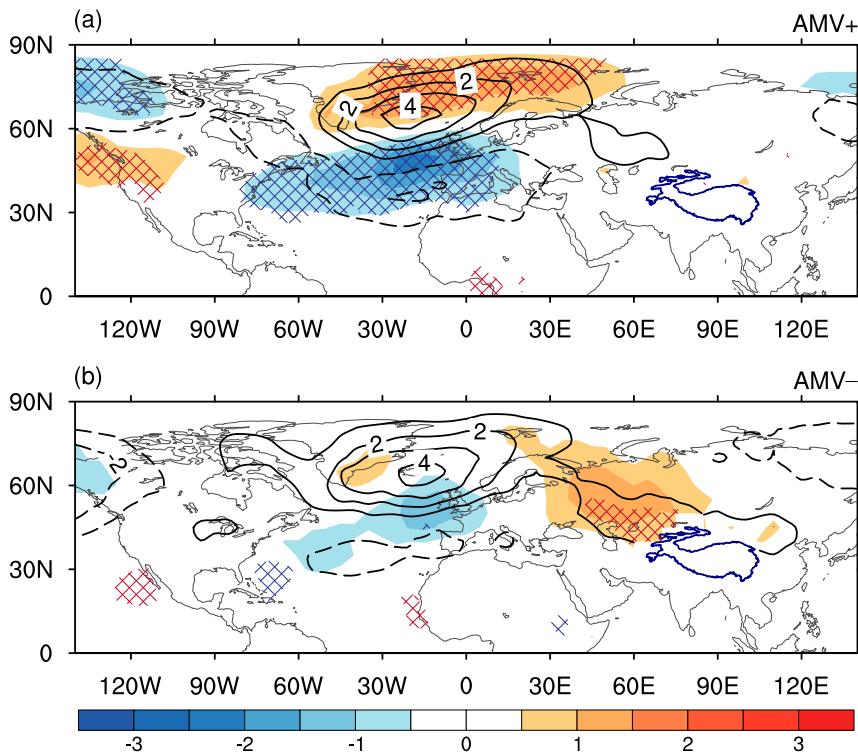

FIG. 3. Regressions of deviation from the zonal-mean SLP in February (contours; hPa) and in March (shading; hPa) upon the negative February NAO index during (a) the warm AMV phase and (b) the cold AMV phase. Cross-hatched regions hereinafter denote values that are significant at 95% confidence level from a two-tailed Student's *t* test.
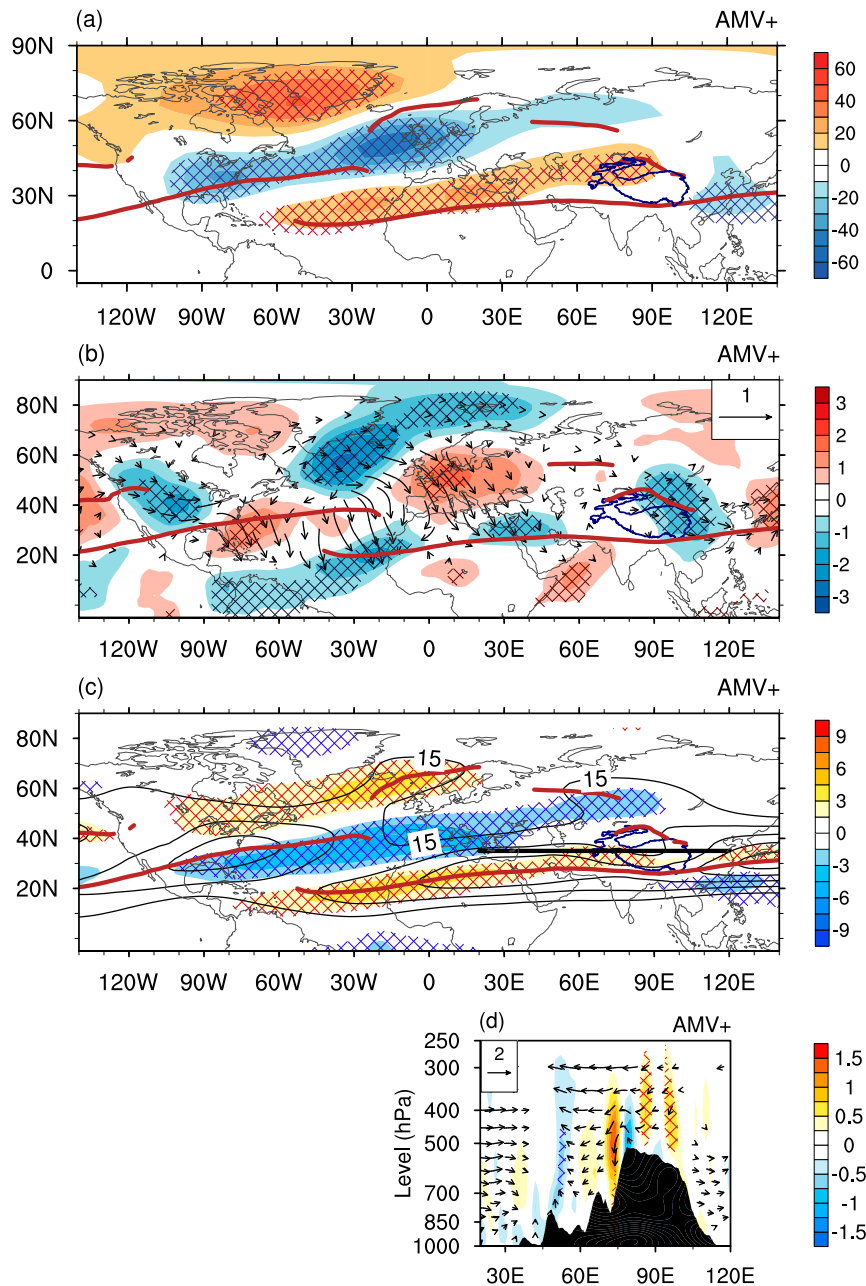
FIG. 4. Regressions of 250-hPa (a) geopotential height (shading; 10 gpm), (b) meridional wind (shading; m s^{-1}) and WAFs (vectors; m^2 s^{-2}), (c) zonal wind (shading; m s^{-1}) and its climatology (contours; m s^{-1}), and (d) omega (shading; 10^{-2} Pa s^{-1}) and zonal–vertical (omega) winds (vectors; m s^{-1} and 10^{-2} Pa s^{-1} in zonal and vertical directions, respectively) cross section (longitude vs pressure) along 35°N [denoted by the thick line in (c)] in March upon the negative February NAO index during the warm AMV phase. Brown thick curves in (a)–(c) denote the climatological westerly jet axes at 250 hPa during the warm AMV phase.

is a positive (negative) geopotential height anomaly over the polar cap (midlatitude North Atlantic) in the upper troposphere (Fig. 4a), in accordance with the NAO− in the SLP field (Fig. 3a, shading). Additionally, a high anomaly originates from the eastern North Atlantic and extends along the

subtropical westerly jet stream across Eurasia followed by a low anomaly downstream, disturbing circulation over the TP and East Asia, respectively. A close investigation of 250-hPa meridional winds and associated WAFs further indicates that clear RWTs are emitted from the North Atlantic and mainly
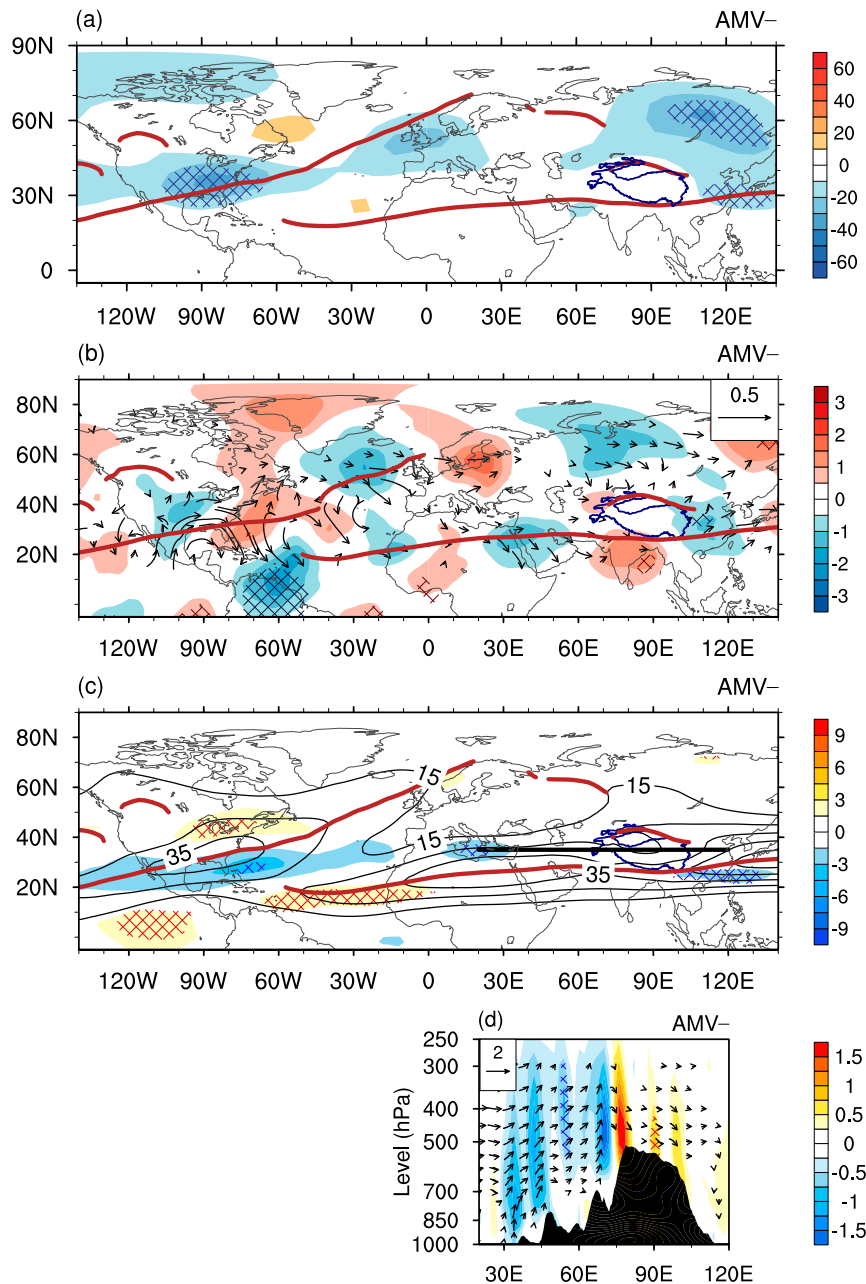
FIG. 5. As in Fig. 4, but for the cold AMV phase.

propagate along the subtropical westerly waveguide toward the TP (Fig. 4b). In the 250-hPa zonal wind field, there is a negative (positive) anomaly at 30°N (45°N) across Eurasia, which extends eastward toward the southern (northern) flank of the TP (Fig. 4c, shading) and induces a deceleration and northward shift of the overlying westerly jet. Correspondingly, the vertical profile of winds along 35°N illustrates a significant subsidence anomaly over the TP (Fig. 4d, shading), indicative of a simultaneous secondary circulation anomaly that occurs in March. Moreover, over East Asia, the negative (positive) zonal wind anomaly at 30°N (20°N) implies a southward-shifted

westerly jet. The negative zonal wind anomaly at 50°N concurrent with the positive anomaly at 30°N over the North Atlantic–Europe sector during NAO− reinforces the deceleration of subtropical and polar-front jet streams in March (Fig. 4c, shading), especially over the Atlantic where they tend to merge and become nearly zonally oriented (see Fig. S1a in the online supplemental material).

During the AMV−, however, the upper-troposphere circulation anomaly over the North Atlantic is much weaker in March despite a low anomaly over eastern North America (Fig. 5a). Instead, concurrent with the eastward-propagating
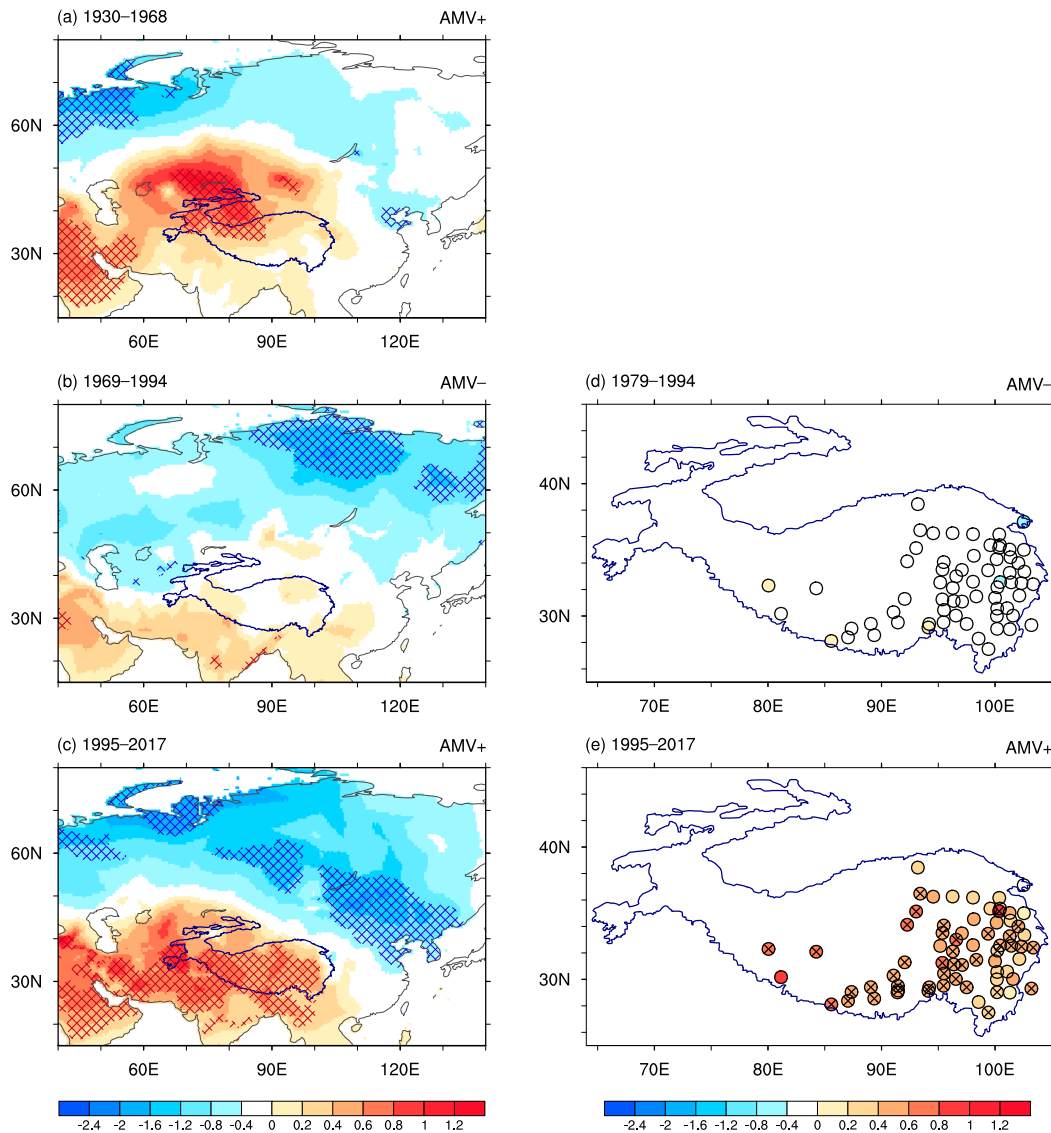
FIG. 6. (a)–(c) Regressions of SAT (°C) in March upon the negative February NAO index during (a) 1930–68 (the warm AMV phase), (b) 1969–94 (the cold AMV phase), and (c) 1995−2017 (the warm AMV phase). (d),(e) As in (a)–(c), but for station-based observation in the period of 1979–2017. Circles with crosses denote values that are significant at 95% confidence level from a two-tailed Student's t test.

SLP anomaly in March (Fig. 3b, shading), there appear two separate trains of alternative negative and positive 250-hPa meridional wind anomalies along the polar-front jet stream over high-latitude Eurasia (although it is less significant) and the subtropical jet stream south of the TP, respectively (Fig. 5b and Fig. S1b). Little response occurs in wind fields over the TP (Figs. 5c,d), demonstrating that the subtropical RWT during the AMV− exerts little impact on circulation variability over the TP.

The response of SAT in March is then analyzed separately in 1930–68 (AMV+), 1969–94 (AMV−), and 1995–2017 (AMV+) to compare with the station-based observation from the period of 1979–2017. As shown in Figs. 6a and 6c, in

accordance with the anomalous descending motion that intensifies adiabatic heating over the TP during the AMV+ (Fig. 4d), there appears to be a positive SAT anomaly from the Arabian Peninsula to the TP (15°–40°N) in March, although that in 1930–68 tends to be concentrated over the western TP. Nevertheless, there is little SAT response over the TP during the AMV− (Fig. 6b). The regression based on station data reinforces this conclusion, illustrating that NAO− is significantly correlated with an enhanced TPSAT in March during the AMV+ (Fig. 6e) but shows no association during the AMV− (Fig. 6d). In addition, a negative SAT anomaly is observed over midlatitude Eurasia during both AMV phases (Figs. 6a–c), which should be related to the low anomaly there
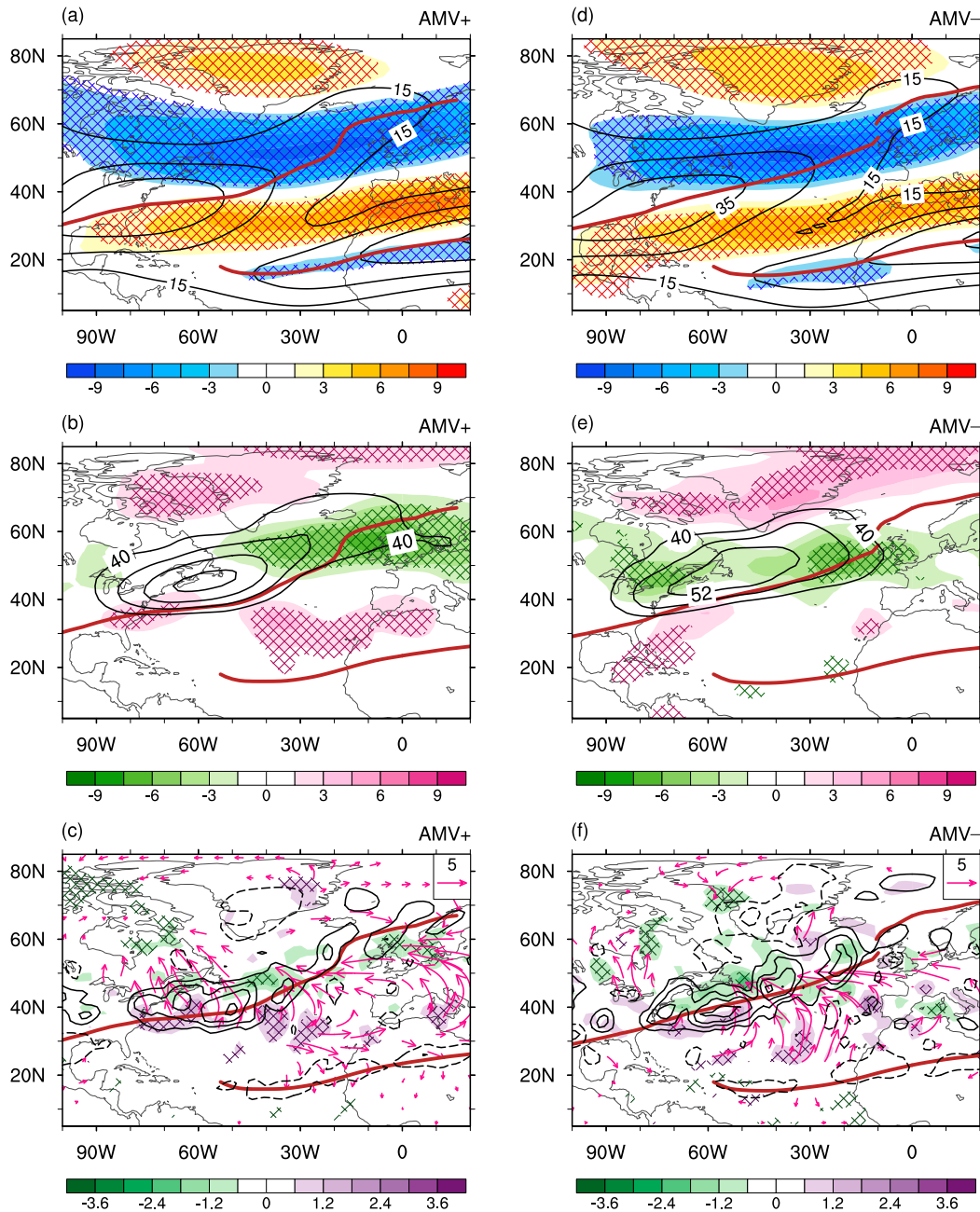
FIG. 7. Climatology (contours) and regressions (shading) of (a) 250-hPa zonal winds (m s^{-1}), (b) 500-hPa transient eddies (10 gpm), and (c) 250-hPa localized E-P flux (**E**; vectors; m^2 s^{-2}) and its divergence (m s^{-1} day^{-1}) in February upon the negative February NAO index during the warm AMV phase. (d)–(f) As in (a)–(c), but for the cold AMV phase. Brown thick curves denote the climatological westerly jet axes at 250 hPa in each AMV phases.

(Figs. 4a and 5a). The strengthened East Asian trough and southward-shifted East Asia westerly jet during the AMV+ (Figs. 4a,c) are responsible for the additional atmospheric cooling over East Asia.

In conclusion, during the AMV+, the NAO− in February could persist into March, accompanied by a stationary RWT propagating along the subtropical westerly waveguide across

Eurasia, which induces a deceleration and a northward shift of the westerly jet stream over the TP. Accordingly, an anomalous descending motion over the TP warms the local air via enhanced adiabatic heating. However, during the AMV−, the circulation anomaly over the North Atlantic diminishes and moves downstream in March, in which the positive SLP anomaly related to the NAO− over Iceland in February is
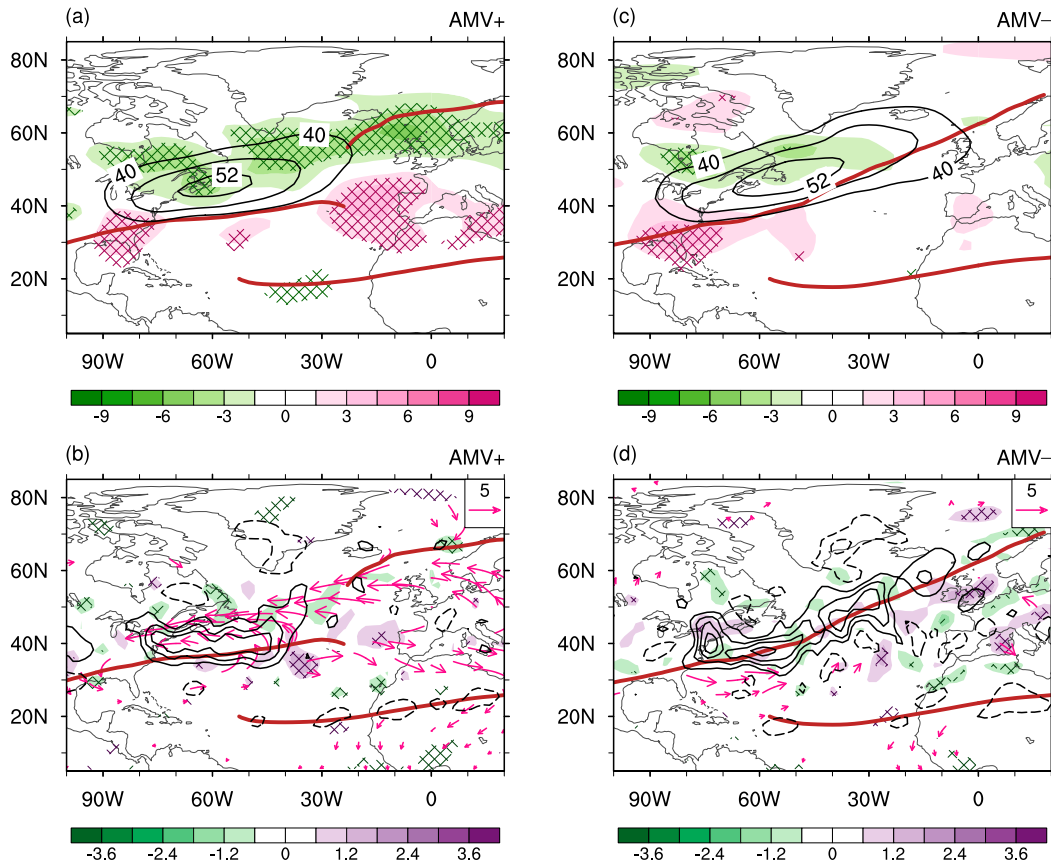
FIG. 8. Climatology (contours) and regressions (shading) of (a) 500-hPa transient eddies (10 gpm) and (b) 250-hPa localized E-P flux (**E**; vectors; $m^2 s^{-2}$) and its divergence ($m s^{-1} day^{-1}$) in March upon the negative February NAO index during the warm AMV phase. (c),(d) As in (a) and (b), but for the cold AMV phase. Brown thick curves denote the climatological westerly jet axes at 250 hPa in each AMV phase.

found over northern Europe in March. The upper-level RWTs propagate zonally along the subpolar and subtropical routes across Eurasia, and the latter travels well south of the TP, exerting no impact on TPSAT variability in March.

c. The potential modulation of the AMV upon SELF feedback to the NAO flow

Then, the question arises as to why an NAO− could persist from February to March during the AMV+ and impact the TPSAT in March by triggering a stationary RWT, while RWTs excited along the subpolar and subtropical routes during the AMV− have no impact on TPSAT. Since the SELF interaction plays an important role in maintaining the NAO flow via positive eddy feedback, it is further examined under each AMV phase.

The regressions of the 250-hPa zonal winds, 500-hPa transient eddies, and 250-hPa localized E-P flux (**E**) on the negative February NAO index are first taken during the AMV+ and the AMV−. When NAO− occurs in February, the 250-hPa zonal wind field exhibits near zonally uniform positive and negative anomalies at 30° and 50°N across the North Atlantic–western European region during both AMV phases (Figs. 7a,d),

indicating a decelerated subtropical jet and polar-front jet concurrent with the NAO−. The 500-hPa transient eddies also show a meridional dipole of positive and negative anomalies south (30°N) and north (50°N) of the climatological center, but the positive anomaly over the subtropical North Atlantic during the AMV+ (Fig. 7b) is much more robust than that during the AMV− (Fig. 7e). The dipole of the transient eddy anomaly indicates the equatorward shift of the Atlantic storm track. Meanwhile, the **E** vectors consistently show easterly convergent anomalies at 50°N and westerly divergent anomalies at 30°N in February during both AMV phases (Figs. 7c,f), favoring local westerly deceleration and acceleration, respectively. This result further suggests that the equatorward-shifted storm track favors westerly shifting more southward and thus exerts a positive feedback upon the NAO− flow. However, a difference occurs in the south of the mean storm track location at 30°N over the eastern North Atlantic, where robust westerly divergent **E** vectors appear during the AMV+ (Fig. 7c: vectors) but do not appear during the AMV− (Fig. 7f: vectors). The divergence of **E** also exhibits a stronger positive anomaly at 30°N during the AMV+ (Fig. 7c: shading), which implies a stronger SELF interaction over the subtropical North Atlantic
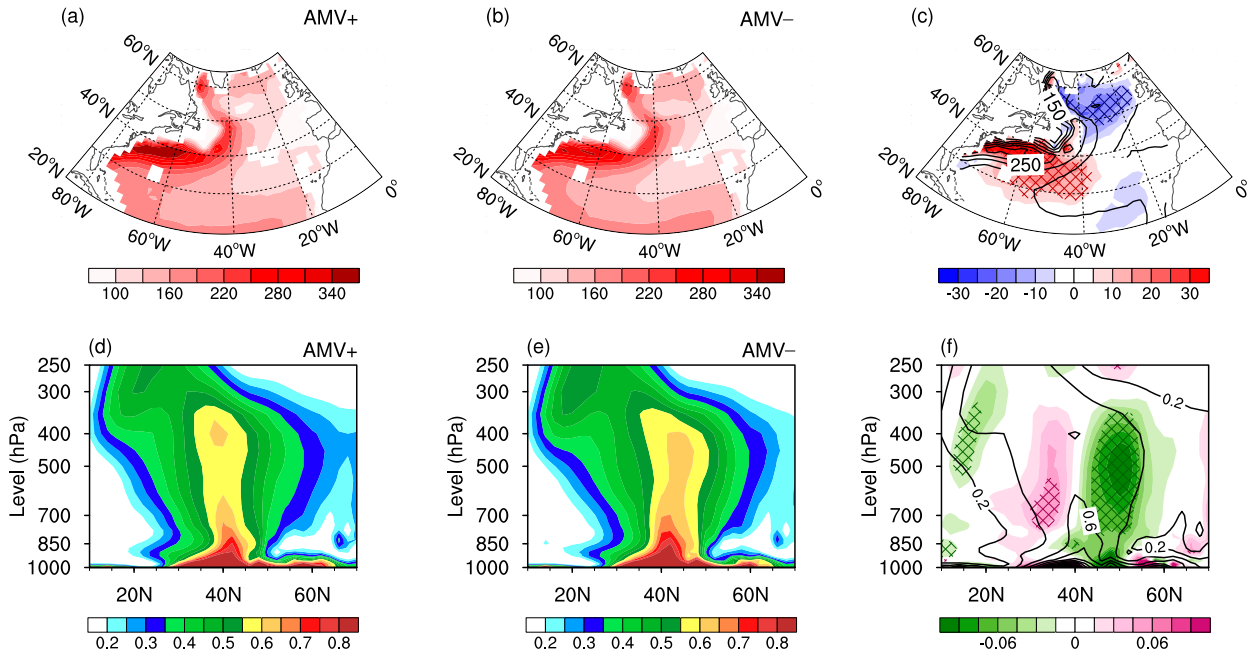
FIG. 9. (a)–(c) Climatology of surface turbulent heat flux (sum of sensible and latent heat fluxes with positive indicating upward direction; W m^{-2}) averaged in February–March (10 gpm) during (a) the warm AMV phase and (b) the cold AMV phase, and (c) their difference (shading; variables during the warm AMV phase minus those during the cold AMV phase). (d)–(f) As in (a)–(c), but for the Eady growth rate (day^{-1}) along 55°W. Contours in (c) and (f) are the climatology for the full record.

Ocean during the AMV+. We then compare the standard deviation of the SLP over the station of Gibraltar in February during different AMV phases, finding that variability during the AMV+ (4.05 hPa) is significantly larger than that during the AMV− (3.08 hPa; over the 90% confidence level based on an F test). This result suggests that the interannual variability of the North Atlantic subtropical high in February during the AMV+ should be stronger than that during the AMV−, which could be partially associated with the stronger SELF interaction.

In the following March during the AMV+, there are still positive and negative 500-hPa transient eddy anomalies across the North Atlantic at 30° and 50°N, respectively (Fig. 8a), accompanied by westerly divergent and easterly convergent **E** vectors in situ (Fig. 8b), which exert positive feedbacks on the NAO− flow by accelerating (decelerating) zonal winds at 30°N (50°N) (Figs. 4c and 8b, shading). The atmospheric structure in March is similar to that in February, representing an NAO− with SELF feedback for 2 months during the AMV+. However, during the AMV−, the meridional dipole of transient eddy anomalies largely diminishes in March (Fig. 8c), suggesting little covariability of synoptic fluctuations and time-mean flow over the North Atlantic. Consequently, small-amplitude **E** vectors are observed during the AMV− (Fig. 8d), and the zonal wind anomaly disappears with the absence of the SELF feedback (Fig. 5c). The diminished NAO− flow in March during the AMV− agrees with the observed weakened and downstream-propagated circulation anomaly depicted in Figs. 3b and 5.

As mentioned above, the AMV footprint is found in multidecadal fluctuations of intraseasonal circulations, especially over the North Atlantic. For instance, during the AMV+, the

subtropical westerly jet stream accelerates due to North Atlantic warming, while the storm track shifts equatorward because of the corresponding southward shift in atmospheric maximum baroclinicity, as proven by the numerical experiments in Peings and Magnusdottir (2014) and Msadek et al. (2010). To estimate the influence of the AMV on the SELF interaction, the climatology of the February–March surface turbulent heat flux and the vertical profile of the Eady growth rate over the western North Atlantic along 55°W are shown during the AMV+, the AMV−, and as a composite difference (Fig. 9). Climatologically, the maximum turbulent heat flux warming the atmosphere is found in the Gulf Stream (Figs. 9a,b). Additionally, the Atlantic storm track emerges in this region due to the strong land–sea thermal contrast and high baroclinicity in the atmosphere (Figs. 9d,e; Brayshaw et al. 2011). The ocean releases more energy to the atmosphere during AMV+ than during AMV− through the above-normal turbulent heat flux anomaly in the climatological center at 40°N (Fig. 9c: shading; Häkkinen et al. 2011; Zhang et al. 2019). This process induces a southward displacement of the overlying atmospheric baroclinicity due to the positive/negative anomalies to the south/north of the climatological center of the Eady growth rate (Fig. 9f: shading).

Figure 10 is the same as Fig. 9, except for the 500-Pa transient eddy activity, 250-hPa localized E-P flux, and zonal winds. The storm track is centered over the western North Atlantic at ~45° and 50°N during the AMV+ and the AMV−, respectively, and it extends northeastward toward the eastern North Atlantic (Figs. 10a,b). Their composite difference demonstrates that, consistent with the southward-shifted atmospheric
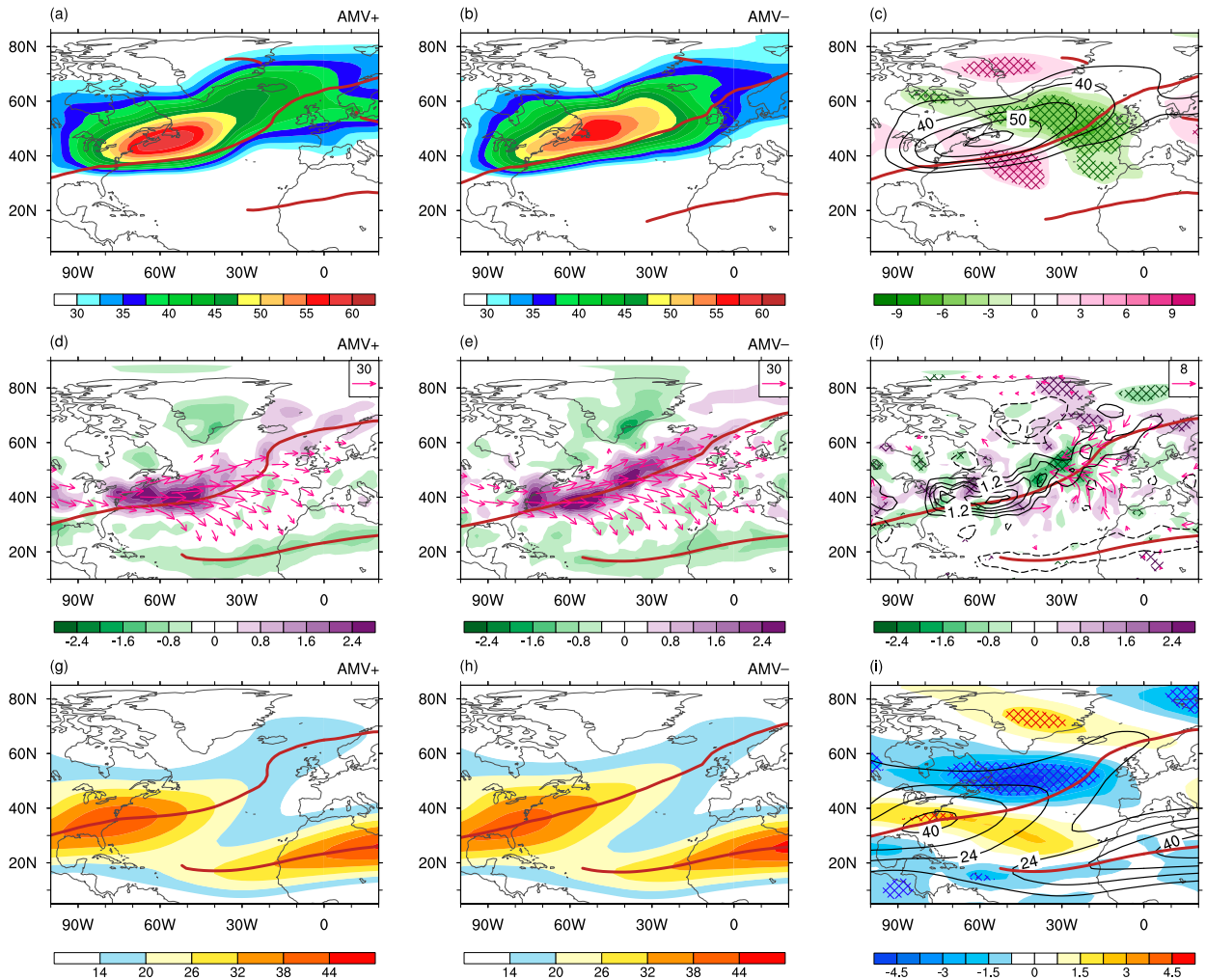
FIG. 10. (a)–(c) Climatology of 500-hPa transient eddies averaged in February–March (10 gpm) during (a) the warm AMV phase and (b) the cold AMV phase, and (c) their difference (shading; variables during the warm AMV phase minus those during the cold AMV phase). (d)–(f) As in (a)–(c), but for 250-hPa localized E-P flux (**E**; vectors; $m^2\,s^{-2}$) and its divergence (shading; $m\,s^{-1}\,day^{-1}$). (g)–(i) As in (a)–(c), but for 250-hPa zonal winds ($m\,s^{-1}$). Contours in (c), (f), and (j) are the climatology for the full record. Brown thick curves denote the climatological westerly jet axes at 250 hPa in each AMV phase, while those in (c), (f), and (j) are the time mean in 1920–2017.

baroclinicity shown in Fig. 9f, there appears to be a dipole pattern in the transient eddy anomaly around its climatological center (Fig. 10c): an increase and a decrease occur along 35° and 50°N, respectively. These results thus indicate that the Atlantic storm track is located more equatorward during the AMV+ than the AMV−, especially in its climatological maximum over the western North Atlantic; additionally, its northeastward extension into the eastern North Atlantic is also more limited. On the other hand, a similar dipole anomaly pattern in the divergence of **E** is apparent (Fig. 10f): the divergence of **E** is enhanced along 40°N over the climatological maximum, with a negative anomaly to the north, indicating enhanced (suppressed) SELF feedback along the subtropical (polar front) westerly jet stream over the North Atlantic. In the climatological field, the **E** vectors in February–March are more zonally oriented with comparably stronger centers over the

subtropical North Atlantic during the AMV+ (Fig. 10d), while they extend much more northeastward toward the eastern North Atlantic during the AMV− (Fig. 10e). As expected, the subtropical westerly jet stream over the North Atlantic is strengthened and more zonally oriented, and its northeastward extension is more limited during the AMV+ (Fig. 10g) than that in the AMV− (Fig. 10h). The composite difference of the 250-hPa zonal winds between the AMV+ and the AMV− further indicates that the AMV+ is concurrent with an acceleration of the North Atlantic subtropical westerly jet and deceleration of the polar-front jet compared with those during the AMV− (Fig. 10i), which reconciles with the changes in SELF interaction (Fig. 10f).

In summary, during the AMV+, the NAO− is closely linked to the SELF interaction over the North Atlantic in both February and March, exerting positive feedback to maintain
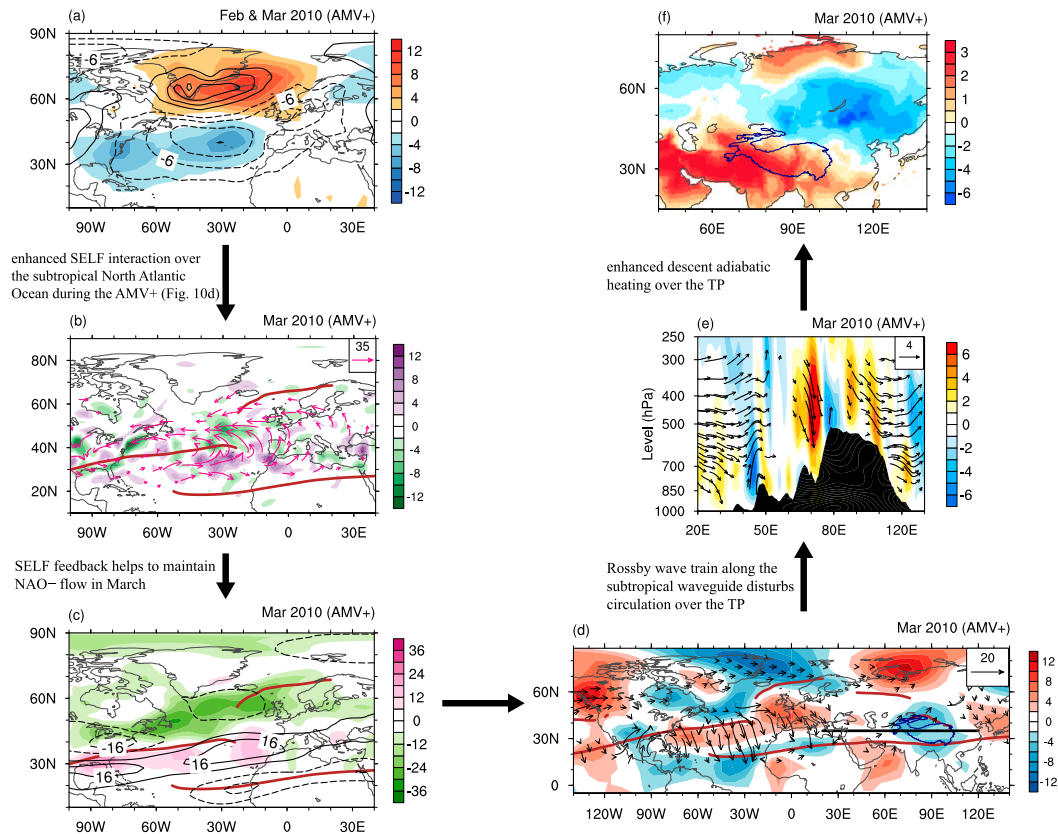
FIG. 11. Case study associated with extreme negative NAO event in February 2010. Observed anomalies of (a) deviation from the zonal-mean SLP in February 2010 (contours; hPa) and in March 2010 (shading; hPa), (b) 250-hPa localized E-P flux (**E**; vectors; $m^2 s^{-2}$) and its divergence (shading; $m s^{-1} day^{-1}$) in March 2010, (c) 500-hPa transient eddies (shading; 10 gpm) and 250-hPa zonal winds (contours; $m s^{-1}$) in March 2010, (d) 250-hPa meridional winds (shading; $m s^{-1}$) and WAFs (vectors; $m^2 s^{-2}$) in March 2010, (e) omega (shading; $10^{-2} Pa s^{-1}$) and zonal–vertical (omega) winds (vectors; $m s^{-1}$ and $10^{-2} Pa s^{-1}$ in zonal and vertical directions, respectively) cross section along 35°N [denoted by the black thick line in (d)] in March 2010, and (f) SAT (°C) in March 2010. Brown thick curves in (b)–(d) denote the climatological westerly jet axes at 250 hPa during the warm AMV phase.

the NAO− pattern in March. However, during the AMV−, the NAO− coincides with comparably weaker SELF feedback in February, especially over the subtropical North Atlantic, which diminishes in the following March. The stronger SELF interaction during the AMV+ might result from a southward-shifted Atlantic storm track caused by positive SST anomalies associated with the AMV+, which enhances the climatological eddy forcing center on the time-mean flow along 40°N over the North Atlantic.

4. Discussion and summary

This study investigated the multidecadal modulation of the AMV on the connection between the February NAO and March TPSAT. A better understanding of the mechanism can be obtained by contrasting analyses of two extreme NAO− events that stand out in Fig. 1b during separate AMV phases. There is a long-duration extreme event of NAO− from December 2009 to March 2010, with the second largest magnitude on record since 1920 (Figs. 1b and 11a; Osborn 2011;

Cohen et al. 2010). Under the background of the AMV+, there is an obvious positive eddy feedback upon the NAO− flow in March 2010: on the one hand, the SELF interaction, reflected by the robust positive (negative) anomalies in divergence of **E**, appears along 30°N (50°N) (Fig. 11b), favoring the westerly acceleration (deceleration) in situ, and displacing the Atlantic westerly jet stream equatorward. On the other hand, the equatorward-shifted westerly jet stream guides the Atlantic storm track more southward, and the covariability of the transient eddies and the time-mean flow reinforces the SELF interaction in March (Fig. 11c). As expected, in March 2010, a Rossby wave train originates from the North Atlantic and propagates along the subtropical westerly waveguide in Eurasia eastward toward the TP (Fig. 11d). Correspondingly, anomalous descending motions are observed over the TP (Fig. 11e), which lead to regional positive SAT anomaly in March 2010 (Fig. 11f).

Another extreme event of NAO− in February 1986 is characterized by the third largest magnitude on record (Figs. 1b and 12a). In March 1986, under the background of
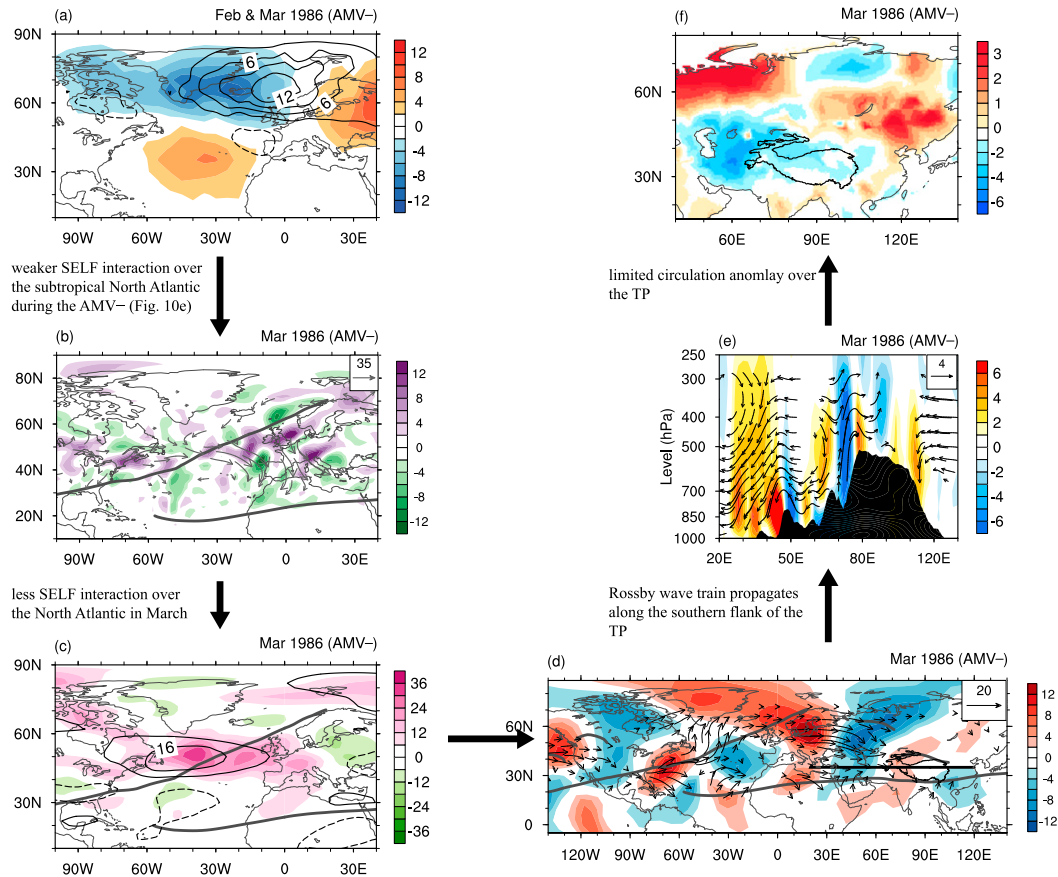
FIG. 12. As in Fig. 11, but for a case study of an extreme negative NAO event in February 1986.

AMV−, there is weak SELF interaction over the North Atlantic, although some westerly divergent **E** vectors prevail along 50°N (Fig. 12b). Meanwhile, the atmospheric structure related to NAO− in February 1986 was replaced by a positive anomaly of transient eddies and 250-hPa zonal winds at 50°N in March 1986 (Fig. 12c), implying the downstream propagation of the circulation anomaly. Accordingly, RWTs propagated in both the subpolar and the subtropical routes, traveling along the northern and southern flanks of the TP but exerting little impact on the TP in March 1986 (Fig. 12d). The NAO− event in February 1986 thus showed no association with the TP circulation and temperature variations in the following month (Figs. 12e,f).

This study suggests that the reinforcement of the SELF interaction in the climatological maximum over the subtropical North Atlantic in February and March during the AMV+ is crucial for conveying NAO signals to the TP. On the one hand, the stronger SELF interaction tends to strengthen the subtropical high over the North Atlantic in February, contributing to a stronger NAO− pattern. On the other hand, it plays an important role in maintaining the NAO− flow into the following March via positive eddy feedback, which triggers a stationary RWT and further influences the TP, as illustrated in Fig. 11. We further attribute SELF interaction changes to AMV-related atmospheric response over the Gulf Stream,

where the oceanic intrinsic processes at multidecadal time scales contribute to the AMV via meridional heat transport (Zhang et al. 2019). The turbulent heat flux over the Gulf Stream during the AMV+ is significantly enhanced compared to the AMV− (Figs. 9a–c), suggesting that the ocean releases more heat into the atmosphere aloft. Such increased oceanic heating is found to shift the storm track more southward by disturbing local atmospheric baroclinicity, leading to strengthened SELF interaction over the subtropical North Atlantic in 40°N. To confirm the results on the climate impacts of the AMV, composite maps are created by using ERA-20C (1920–2010; Figs. S2 and S3). The results were broadly similar to the corresponding fields based on the patched data of ERA-20C and ERA-Interim with the period of 1920–2017, such as enhanced turbulent heat flux over the Gulf Stream, a strengthened and southward-shifted Atlantic storm track, an accelerated subtropical westerly jet, and an enhanced SELF interaction over the midlatitude North Atlantic (Figs. 9 and 10).

A key point to note is that the quasi-stationary RWT mainly propagates along a northward shifted subtropical westerly waveguide across Eurasia in March during the AMV+ (Fig. 4b and Fig. S1a), but while along both the subtropical and subpolar jets during the AMV− (Fig. 5b and Fig. S1b). This key difference finds its root in the variability of the North Atlantic westerly jet: the AMV+ results in a more equatorward-shifted

and zonally oriented westerly maximum over the North Atlantic–Europe sector particularly in March, which is more likely to convey the NAO signals along the subtropical waveguide, a result also found in Simpson et al. (2018) and Simpson et al. (2019); whereas the more tilted North Atlantic jet stream during the AMV− might favor the RWTs propagating along the well-separated subpolar and subtropical routes. This RWT propagation conveying NAO signals across Eurasia is also relevant later in the summer season, when the so-called Silk Road pattern is trapped along a weakened subtropical on the northern flank of the TP (Liu and Yin 2001; Gao et al. 2013; He et al. 2018; Orsolini et al. 2015). Further analysis would be necessary to examine in detail these teleconnections in other seasons.

REFERENCES

Allan, R., and T. Ansell, 2006: A new globally complete monthly historical gridded mean sea level pressure dataset (HadSLP2): 1850–2004. *J. Climate*, **19**, 5816–5842, https://doi.org/10.1175/JCLI3937.1.

Bao, Q., J. Yang and Y. Liu, 2010: Roles of anomalous Tibetan Plateau warming on the severe 2008 winter storm in central-southern China. *Mon. Wea. Rev.*, **138**, 2375–2384, https://doi.org/10.1175/2009MWR2950.1.

Bao, Y., and Q. You, 2019: How do westerly jet streams regulate the winter snow depth over the Tibetan Plateau? *Climate. Dyn.*, **53**, 353–370, https://doi.org/10.1007/S00382-018-4589-1.

Brayshaw, D. J., B. Hoskins, and M. Blackburn, 2011: The basic ingredients of the North Atlantic storm track. Part II: Sea surface temperatures. *J. Atmos. Sci.*, **68**, 1784–1805, https://doi.org/10.1175/2011JAS3674.1.

Chen, L., R. Zhang, S. C. Pryor, X. Li, and H. Wang, 2020: Influence of wintertime surface sensible heat flux variability over the central and eastern Tibetan Plateau on the East Asian winter monsoon. *Climate Dyn.*, **54**, 4589–4603, https://doi.org/10.1007/s00382-020-05246-x.

Cohen, J., J. Foster, M. Barlow, K. Saito, and J. Jones, 2010: Winter 2009–2010: A case study of an extreme Arctic Oscillation event. *Geophys. Res. Lett.*, **37**, L17707, https://doi.org/10.1029/2010GL044256.

Dee, D. P., and Coauthors, 2011: The ERA-Interim reanalysis: Configuration and performance of the data assimilation system. *Quart. J. Roy. Meteor. Soc.*, **137**, 553–597, https://doi.org/10.1002/qj.828.

Gao, J., M. W. Williams, X. Fu, G. Wang, and T. Gong, 2012: Spatiotemporal distribution of snow in eastern Tibet and the

response to climate change. *Remote Sens. Environ.*, **121**, 1–9, https://doi.org/10.1016/j.rse.2012.01.006.

Gao, Y., H. Wang, and S. Li, 2013: Influences of the Atlantic Ocean on the summer precipitation of the southeastern Tibetan Plateau. *J. Geophys. Res. Atmos.*, **118**, 3534–3544, https://doi.org/10.1002/jgrd.50290.

Guo, D., E. Yu, and H. Wang, 2016: Will the Tibetan Plateau warming depend on elevation in the future? *J. Geophys. Res. Atmos.*, **121**, 3969–3978, https://doi.org/10.1002/2016JD024871.

Häkkinen, S., P. B. Rhines, and D. L. Worthen, 2011: Atmospheric blocking and Atlantic multidecadal ocean variability. *Science*, **334**, 655–659, https://doi.org/10.1126/science.1205683.

Harris, I., P. D. Jones, T. J. Osborn, and D. H. Lister, 2014: Updated high-resolution grids of monthly climatic observations—The CRU TS3.10 dataset. *Int. J. Climatol.*, **34**, 623–642, https://doi.org/10.1002/joc.3711.

He, S., Y. Gao, T. Furevik, H. Wang, and F. Li, 2018: Teleconnection between sea ice in the Barents Sea in June and the Silk Road, Pacific–Japan and East Asian rainfall patterns in August. *Adv. Atmos. Sci.*, **35**, 52–64, https://doi.org/10.1007/s00376-017-7029-y.

Hoskins, B. J., I. N. James, and G. H. White, 1983: The shape, propagation and mean-flow interaction of large-scale weather systems. *J. Atmos. Sci.*, **40**, 1592–1612, https://doi.org/10.1175/1520-0469(1983)040<1595:TSPAMF>2.0.CO;2.

Hurrell, J. W., 2003: An overview of the North Atlantic Oscillation. *The North Atlantic Oscillation—Climate Significance and Environmental Impact, Geophys. Monogr.,* Vol. 134, Amer. Geophys. Union, 1–35.

Imtiaz, R., R. J. Miller, L. G. Russell, and M. Xu, 2009: Using a global climate model to evaluate the influences of water vapor, snow cover and atmospheric aerosol on warming in the Tibetan Plateau during the twenty-first century. *Climate Dyn.*, **34**, 859–872, https://doi.org/10.1007/S00382-009-0564-1.

IPCC, 2014: *Climate Change 2014: Synthesis Report.* Cambridge University Press, 151 pp.

Jones, P. D., T. Jónsson, and D. Wheeler, 1997: Extension to the North Atlantic Oscillation using early instrumental pressure observations from Gibraltar and south-west Iceland. *Int. J. Climatol.*, **17**, 1433–1450, https://doi.org/10.1002/(SICI)1097-0088(19971115)17:13<1433::AID-JOC203>3.0.CO;2-P.

Kerr, R., 2000: A North Atlantic climate pacemaker for the centuries. *Science*, **288**, 1984–1985, https://doi.org/10.1126/science.288.5473.1984.

Lau, N. C., 1988: Variability of the observed midlatitude storm tracks in relation to low-frequency changes in the circulation pattern. *J. Atmos. Sci.*, **45**, 2718–2743, https://doi.org/10.1175/1520-0469(1988)045<2718:VOTOMS>2.0.CO;2.

——, and M. J. Nath, 1991: Variability of the baroclinic and barotropic transient eddy forcing associated with monthly changes in the midlatitude storm tracks. *J. Atmos. Sci.*, **48**, 2589–2613, https://doi.org/10.1175/1520-0469(1991)048<2589:VOTBAB>2.0.CO;2.

Li, J., R. Yu, T. Zhou, and B. Wang, 2005: Why is there an early spring cooling shift downstream of the Tibetan Plateau? *J. Climate*, **18**, 4660–4668, https://doi.org/10.1175/JCLI3568.1.

——, ——, and ——, 2008: Teleconnection between NAO and climate downstream of the Tibetan Plateau. *J. Climate*, **21**, 4680–4690, https://doi.org/10.1175/2008JCLI2053.1.

Li, L., S. Yang, Z. Wang, X. Zhu, and H. Tang 2010: Evidence of warming and wetting climate over the Qinghai-Tibet Plateau. *Arct. Antarct. Alp. Res.*, **42**, 449–457, https://doi.org/10.1657/1938-4246-42.4.449.

Liu, X., and B. Chen, 2000: Climatic warming in the Tibetan Plateau during recent decades. *Int. J. Climatol.*, **20**, 1729–1742,

https://doi.org/10.1002/1097-0088(20001130)20:14<1729::AID-JOC556>3.0.CO;2-Y.

——, and Z. Yin, 2001: Spatial and temporal variation of summer precipitation over the eastern Tibetan Plateau and the North Atlantic Oscillation. *J. Climate*, **14**, 2896–2909, https://doi.org/10.1175/1520-0442(2001)014<2896:SATVOS>2.0.CO;2.

Maurer, J. M., J. M. Schaefer, S. Rupper, and A. Corley, 2019: Acceleration of ice loss across the Himalayas over the past 40 years. *Sci. Adv.*, **5**, eaav7266, https://doi.org/10.1126/sciadv.aav7266.

Msadek, R., C. Frankignoul, and L. Z. X. Li, 2010: Mechanisms of the atmospheric response to North Atlantic multidecadal variability: A model study. *Climate Dyn.*, **36**, 1255–1276, https://doi.org/10.1007/s00382-010-0958-0.

Orsolini, Y. J., L. Zhang, and H. W. Dieter, 2015: Extreme precipitation events over North China in August 2010 and their link to eastward-propagating wave-trains across Eurasia: Observations and monthly forecasting. *Quart. J. Roy. Meteor. Soc.*, **141**, 3097–3105, https://doi.org/10.1002/qj.2594.

Osborn, T. J., 2011: Winter 2009/2010 temperatures and a record-breaking North Atlantic Oscillation index. *Weather*, **66**, 19–21, https://doi.org/10.1002/WEA.660.

Palazzi, E., L. Filippi, and J. V. Hardenberg, 2017: Insights into elevation-dependent warming in the Tibetan Plateau–Himalayas from CMIP5 model simulations. *Climate Dyn.*, **48**, 3991–4008, https://doi.org/10.1007/s00382-016-3316-z.

Pan, L., and F. Jin, 2005: Seasonality of synoptic eddy feedback and the AO/NAO. *Geophys. Res. Lett.*, **32**, L21708, https://doi.org/10.1029/2005GL024133.

Peings, Y., and G. Magnusdottir, 2014: Forcing of the wintertime atmospheric circulation by the multidecadal fluctuations of the North Atlantic Ocean. *Environ. Res. Lett.*, **9**, 034018, https://doi.org/10.1088/1748-9326/9/3/034018.

Pepin, N., and Coauthors, 2015: Elevation-dependent warming in mountain regions of the world. *Nat. Climate Change*, **5**, 424–430, https://doi.org/10.1038/nclimate2563.

Poli, P., and Coauthors, 2016: ERA-20C: An atmospheric reanalysis of the twentieth century. *J. Climate*, **29**, 4083–4097, https://doi.org/10.1175/JCLI-D-15-0556.1.

Ramanathan, V., and G. Carmichael, 2008: Global and regional climate changes due to black carbon. *Nat. Geosci.*, **1**, 221–227, https://doi.org/10.1038/ngeo156.

Rayner, N. A., D. E. Parker, E. B. Horton, C. K. Folland, L. V. Alexander, D. P. Rowell, E. C. Kent, and A. Kaplan, 2003: Global analyses of sea surface temperature, sea ice, and night marine air temperature since the late nineteenth century. *J. Geophys. Res.*, **108**, 4407, https://doi.org/10.1029/2002JD002670.

Ren, H., F. Jin, and L. Gao, 2012: Anatomy of synoptic eddy–NAO interaction through eddy structure decomposition. *J. Atmos. Sci.*, **69**, 2171–2191, https://doi.org/10.1175/JAS-D-11-069.1.

Ruprich-Robert, Y., R. Msadek, F. Castruccio, S. Yeager, T. Delworth, and G. Danabasoglu, 2017: Assessing the climate impacts of the observed Atlantic multidecadal variability using the GFDL CM2.1 and NCAR CESM1 global coupled models. *J. Climate*, **30**, 2785–2810, https://doi.org/10.1175/JCLI-D-16-0127.1.

Shen, C., W. C. Wang, and Z. Gang, 2011: Decadal variability in snow cover over the Tibetan Plateau during the last two centuries. *Geophys. Res. Lett.*, **38**, L10703, https://doi.org/10.1029/2011GL047288.

Simpson, I. R., D. Clara, K. A. McKinnon, and E. A. Barnes, 2018: Modeled and observed multidecadal variability in the North Atlantic jet stream and its connection to sea surface temper-

atures. *J. Climate*, **31**, 8313–8338, https://doi.org/10.1175/JCLI-D-18-0168.1.

——, S. Yeager, K. A. McKinnon, and C. Deser, 2019: Decadal predictability of late winter precipitation in western Europe through an ocean-jet stream connection. *Nat. Geosci.*, **12**, 613–619, https://doi.org/10.1038/s41561-019-0391-x.

Su, H., J. Xin, Y. Ma, Z. Liu, and T. Wen, 2018: Effects of transport on aerosols over the eastern slope of the Tibetan Plateau: Synergistic contribution of Southeast Asia and the Sichuan basin. *Atmos. Oceanic Sci. Lett.*, **11**, 425–431, https://doi.org/10.1080/16742834.2018.1512832.

Takaya, K., and H. Nakamura, 2001: A formulation of a phase-independent wave-activity flux for stationary and migratory quasigeostrophic eddies on a zonally varying basic flow. *J. Atmos. Sci.*, **58**, 608–627, https://doi.org/10.1175/1520-0469(2001)058<0608:AFOAPI>2.0.CO;2.

Ting, M., Y. Kushnir, R. Seager, and C. Li, 2009: Forced and internal twentieth-century SST trends in the North Atlantic. *J. Climate*, **22**, 1469–1481, https://doi.org/10.1175/2008JCLI2561.1.

Trenberth, E. K., 1986: An assessment of the impact of transient eddies on the zonal flow during a blocking episode using localized Eliassen–Palm flux diagnostics. *J. Atmos. Sci.*, **43**, 2070–2087, https://doi.org/10.1175/1520-0469(1986)043<2070:AAOTIO>2.0.CO;2.

Vallis, G. K., 2006: *Atmospheric and Oceanic Dynamics: Fundamentals and Large-Scale Circulation.* Cambridge University Press, 745 pp.

Wang, B., Q. Bao, B. Hoskins, G. Wu, and Y. Liu, 2008: Tibetan Plateau warming and precipitation changes in East Asia. *Geophys. Res. Lett.*, **35**, L14702, https://doi.org/10.1029/2008GL034330.

Watanabe, M., 2004: Asian jet waveguide and a downstream extension of the North Atlantic Oscillation. *J. Climate*, **17**, 4674–4691, https://doi.org/10.1175/JCLI-3228.1.

Wu, T., and Z. Qian, 2003: The relation between the Tibetan winter snow and the Asian summer monsoon and rainfall: An observational investigation. *J. Climate*, **16**, 2038–2051, https://doi.org/10.1175/1520-0442(2003)016<2038:TRBTTW>2.0.CO;2.

Xin, X., T. Zhou, and R. Yu, 2010: Increased Tibetan Plateau snow depth: An indicator of the connection between enhanced winter NAO and late-spring tropospheric cooling over East Asia. *Adv. Atmos. Sci.*, **27**, 788–794, https://doi.org/10.1007/s00376-009-9071-x.

Xu, X., C. Lu, X. Shi and S. Gao, 2008: World water tower: An atmospheric perspective. *Geophys. Res. Lett.*, **35**, 525–530, https://doi.org/10.1029/2008GL035867.

——, T. Zhao, C. Lu, and Y. Guo, 2014: An important mechanism sustaining the atmospheric "water tower" over the Tibetan Plateau. *Atmos. Chem. Phys.*, **14**, 11 287–11 295, https://doi.org/10.5194/acp-14-11287-2014.

Yan, Y. F., X. C. Wang, and Y. M. Liu, 2018: Cloud vertical structures associated with precipitation magnitudes over the Tibetan Plateau and its neighboring regions. *Atmos. Oceanic Sci. Lett.*, **11**, 44–53, https://doi.org/10.1080/16742834.2018.1395680.

Yao, T., L. Thompson, and W. Yang, 2012: Different glacier status with atmospheric circulations in Tibetan Plateau and surroundings. *Nature*, **2**, 663–667, https://doi.org/10.1038/nclimate1580.

You, Q., S. Kang, G. Ren, K. Fraedrich, N. Pepin, Y. Yan, and L. Ma, 2011: Observed changes in snow depth and number of snow days in the eastern and central Tibetan Plateau. *Climate Res.*, **46**, 171–183, https://doi.org/10.3354/cr00985.

Yu, H., E. Luedeling, J. Xu, and F. S. Chapin, 2010: Winter and spring warming result in delayed spring phenology on the Tibetan Plateau. *Proc. Natl. Acad. Sci. USA*, **107**, 22 151–22 156, https://doi.org/10.1073/pnas.1012490107.

Zhang, R., R. Sutton, G. Danabasoglu, Y. Kwon, R. Marsh, S. G. Yeager, D. E. Amrhein, and C. M. Little, 2019: A review of the role of the Atlantic meridional overturning circulation in Atlantic multidecadal variability and associated climate impacts. *Rev. Geophys.*, **57**, 316–375, https://doi.org/10.1029/2019RG000644.

Zhang, W., X. Mei, X. Geng, A. G. Turner, and F. Jin, 2018: A nonstationary ENSO–NAO relationship due to AMO mod-ulation. *J. Climate*, **32**, 33–43, https://doi.org/10.1175/JCLI-D-18-0365.1.

Zhang, Y., T. Li, and B. Wang, 2004: Decadal change of the spring snow depth over the Tibetan Plateau: The associated circula-tion and influence on the East Asian summer monsoon. *J. Climate*, **17**, 2780–2793, https://doi.org/10.1175/1520-0442(2004)017<2780:DCOTSS>2.0.CO;2.

Zhu, Y., Y. Ding, and H. Xu, 2008: Decadal relationship between atmospheric heat source and winter-spring snow cover over the Tibetan Plateau and rainfall in East China. *Acta Meteor. Sin.*, **22**, 303–316.